Solar Degradation of Formic Acid: Temperature Effects on the Photo-Fenton Reaction

Jorgelina Farias,[†] Germán H. Rossetti,[†,‡] Enrique D. Albizzati,[‡] and Orlando M. Alfano*[,†]

Instituto de Desarrollo Tecnológico para la Industria Química (INTEC), Consejo Nacional de Investigaciones Científicas y Técnicas (CONICET), and Universidad Nacional del Litoral (UNL), Güemes 3450, 3000 Santa Fe, Argentina, and Facultad de Ingeniería Química, Universidad Nacional del Litoral (UNL), Santiago del Estero 2654, 3000 Santa Fe, Argentina

The effect of the reaction temperature on the degradation rate of formic acid, using the Fenton and photo-Fenton processes, is investigated. First, for both reactions, a stirred tank laboratory photoreactor irradiated from the bottom was used to evaluate the kinetic parameters between 298 and 328 K. Afterward, the proposed kinetic model was used to predict the conversion of the organic pollutant in a flat-plate solar photoreactor. The previously reported radiation field and mass balances have been used to compute the formic acid and hydrogen peroxide concentrations as a function of time in the solar reactor. Theoretical and experimental results show that UV solar radiation improves the effectiveness of the Fenton process. At lower temperatures, the pollutant conversion enhancement is significant, but this effect is less important at higher temperatures. For instance, experimental conversion enhancements after 20 min are 186.0, 74.0, and 7.4% for 298, 313, and 328 K, respectively.

1. Introduction

Advanced oxidation processes (AOPs) have been proposed as an alternative method for the treatment of ground, surface, and waste waters containing toxic and biologically nondegradable organic compounds. These processes, well-known for their capacity for oxidizing and mineralizing a great variety of organic pollutants, are all characterized by the generation of highly reactive hydroxyl radicals (•OH) in the homogeneous or heterogeneous phase.

The Fenton reaction, a mixture of hydrogen peroxide and ferrous salts, is an AOP characterized by the production of hydroxyl radicals in the homogeneous phase at ambient temperature. The production rate of these hydroxyl radicals can be considerably enhanced by irradiating the mixture with UV or UV/visible radiation (the so-called photo-Fenton reaction), improving the degradation rate of various organic contaminants. In recent years, the capability of the photo-Fenton system to destroy most toxic organic compounds at low temperatures has been demonstrated.[1−8]

The feasibility of applying solar radiation as a source of UV/visible radiation has made the photo-Fenton system an economical and competitive process. This solar radiation reaction has been widely proposed to degrade many compounds: EDTA,[9] phenols,[10,11] pesticides,[12−14] surfactants,[15] diclofenac,[16] and other organic compounds.[17]

Recently, it has been shown that an increase of the reaction temperature can enhance the pollutant conversion of the Fenton process.[18−23] A number of attempts have been made applying artificial radiation to study the temperature effect on the photo-Fenton degradation of 4-chlorophenol,[24] Reactive Blue 4,[25] nitrobenzene,[26] and other compounds.[27−29] In the case of the solar photo-Fenton reaction, it was reported the beneficial effect of increased temperature in the oxidative degradation of different aqueous organic pollutants: alachlor,[30] cellulose bleaching effluents,[31,32] and non-biodegradable chlorinated solvents.[33] In addition, an interesting combined photochemical-thermal solar radiation process has been proposed to enhance the reaction rate of the Fenton system to remove an organic pollutant.[34] These authors have developed the so-called insulated solar Fenton hybrid process, on the basis of the use of the entire spectrum of the sun: (i) solar UV/visible energy in the wavelength region 300−500 nm to activate photochemical reactions and (ii) solar thermal energy for wavelengths higher than 500 nm to increase the reaction temperature. A new hybrid photocatalytic−photovoltaic system (HPPS) was also built and investigated, where the UV solar radiation is used for the photocatalytic degradation of biorecalcitrant pollutants and the photovoltaic system is employed to convert the visible solar radiation into electricity.[35]

These contributions were largely involved either in proposing Fenton and/or photo-Fenton kinetic models and reaction mechanisms to evaluate the pollutant decay or in investigating the effects of the reaction temperature on the degradation rate of a specific toxic organic compound. Conversely, in a limited number of studies temperature-dependent kinetic models for both the Fenton and the photo-Fenton reactions, including an explicit formulation for the photon absorption rate inside the solar reactor, have been proposed. In this work, the temperature effects on the Fenton and photo-Fenton degradation rates employing formic acid as a model pollutant are reported. To achieve this goal, the kinetic parameters for a temperature range that goes from 298 to 328 K have been estimated in dark and irradiated laboratory experiments employing a well-stirred tank photoreactor. The reactor was irradiated from the bottom by means of a tubular lamp placed at the focal axis of a cylindrical reflector of parabolic cross section. The activation energies and frequency factors were obtained from a Arrhenius-type diagram for each kinetic parameter.

Afterward, the proposed temperature-dependent kinetic model was used to predict formic acid and hydrogen peroxide

* To whom correspondence should be addressed. Phone: +54-342-4511546. Fax: +54 342 4511087. E-mail: alfano@intec.unl.edu.ar.

[†] Instituto de Desarrollo Tecnológico para la Industria Química (INTEC), Consejo Nacional de Investigaciones Científicas y Técnicas (CONICET), and Universidad Nacional del Litoral (UNL).

[‡] Facultad de Ingeniería Química, Universidad Nacional del Litoral (UNL).

10.1021/ie0700258 CCC: $37.00
Published on Web 05/17/2007

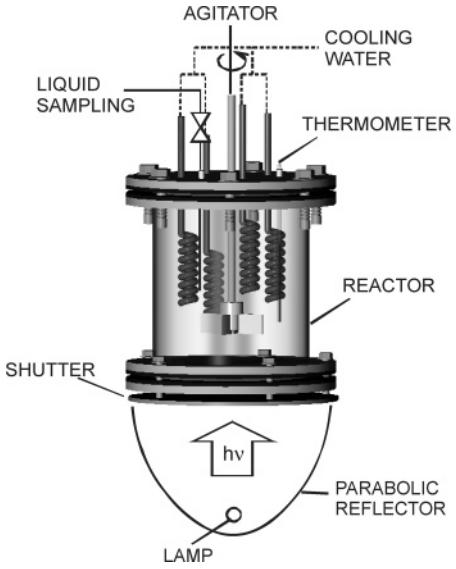

Figure 1. Schematic representation of the stirred tank laboratory photoreactor.

concentrations as a function of time in a flat-plate solar reactor placed inside a batch recycling system. Three reaction temperatures were used for this study: 298, 313, and 328 K. The proposed model is able to account for the dark (Fenton) and the radiation activated (photo-Fenton) reaction rates in a single mathematical expression and to take into account the irradiated and nonirradiated volumes inside the solar reactor. Besides, the local volumetric rate of photon absorption inside the solar reactor has been evaluated, considering the direct and diffuse components of the solar radiation flux incident at the reactor window.

2. Stirred Tank Laboratory Photoreactor

2.1. Reactor Model. Kinetic studies were performed in an isothermal, well-stirred tank photoreactor (Figure 1). A mass balance for the formic acid (F) and the hydrogen peroxide (P) in this batch, perfectly stirred tank photoreactor gives the following set of two nonlinear, first order, ordinary differential equations:

$$\frac{\mathrm{d}C_i(t)}{\mathrm{d}t} = \langle R_i(\mathbf{x}, t)\rangle_{V_R} \quad (i = \mathrm{F}, \mathrm{P}) \tag{1}$$

with the initial conditions

$$t = 0 \quad C_i = C_i^0 \quad (i = \mathrm{F}, \mathrm{P}) \tag{2}$$

The reaction scheme for the photo-Fenton reaction has been described in detail by Pignatello[36] and De Laat and Gallard.[37] The required formic acid (R_F) and hydrogen peroxide (R_P) reaction rates for the mass balances may be obtained from the kinetic model proposed by Rossetti et al.[38]

$$R_{\mathrm{F}}(\mathbf{x}, t) = -\left(\frac{\bar{\Phi} e^{\mathrm{a}}(\mathbf{x}, t)}{1 + K_3(C_{\mathrm{P}}/C_{\mathrm{F}})}\right) + \left(1 + \frac{\bar{\Phi} e^{\mathrm{a}}(\mathbf{x}, t)}{K_4 C_{\mathrm{Fe}^{3+}} C_{\mathrm{P}}}\right)^{1/2} R_{\mathrm{F}}^{\mathrm{t}}(t) \tag{3}$$

$$R_{\mathrm{F}}^{\mathrm{t}}(t) = -\frac{1 + K_2(C_{\mathrm{P}}/C_{\mathrm{Fe}^{3+}})}{1 + K_3(C_{\mathrm{P}}/C_{\mathrm{F}})} K_1 C_{\mathrm{Fe}^{3+}} C_{\mathrm{P}} \tag{4}$$

$$R_{\mathrm{P}}(\mathbf{x}, t) = \left(\frac{\bar{\Phi} e^{\mathrm{a}}(\mathbf{x}, t)}{1 + K_3(C_{\mathrm{P}}/C_{\mathrm{F}})}\right) + \left(1 + \frac{\bar{\Phi} e^{\mathrm{a}}(\mathbf{x}, t)}{K_4 C_{\mathrm{Fe}^{3+}} C_{\mathrm{P}}}\right)^{1/2} R_{\mathrm{P}}^{\mathrm{t}}(t) \tag{5}$$

$$R_{\mathrm{P}}^{\mathrm{t}}(t) = -\left[1 + \frac{1 + K_2(C_{\mathrm{P}}/C_{\mathrm{Fe}^{3+}})}{1 + (C_{\mathrm{F}}/K_3 C_{\mathrm{P}})}\right] K_1 C_{\mathrm{P}} C_{\mathrm{Fe}^{3+}} \tag{6}$$

Here $\bar{\Phi}$ is the wavelength-averaged primary quantum yield, $e^{\mathrm{a}}(\mathbf{x}, t)$ is the local volumetric rate of photon absorption (LVRPA), C_F, C_P, and $C_{Fe^{3+}}$ are the formic acid, hydrogen peroxide, and ferric ion concentrations, and K_i ($i = 1-4$) are the kinetic parameters. Notice that R_F^t and R_P^t are the thermal (or Fenton) formic acid and hydrogen peroxide degradation rates, respectively.

To complete the theoretical description of the kinetic model, it is necessary to introduce the radiation field expression on the right-hand side of eqs 3 and 5. It has been proposed by Alfano et al.[39] that a three-dimensional model should be used to compute the radiation field in a similar photoreactor. These authors proposed and verified experimentally a rigorous radiation model to compute the LVRPA and found that, for restricted optical and geometrical parameters, modifications of the radial and angular coordinates did not introduce significant variations in the radiation field.

In light of these considerations, a one-dimensional radiation field model has been used in this work to calculate the monochromatic LVRPA as a function of the spatial coordinate (x) and the time (t). Thus,

$$e_\lambda^{\mathrm{a}}(x, t) = \kappa_\lambda(t) q_{\mathrm{wall}} f_\lambda \exp[-\kappa_{\mathrm{T},\lambda}(t) x] \tag{7}$$

In eq 7, q_{wall} is the net radiative flux at the wall of the reactor bottom, f_λ is the normalized spectral distribution of the lamp output power provided by the lamp manufacturer, κ_λ the reactant species absorption coefficient, and $\kappa_{T,\lambda}$ is the total absorption coefficient.

According to Faust and Hoigné,[40] the iron complex $Fe(OH)^{2+}$ is the dominant species at pH = 3.0. Furthermore, radiation absorption of hydrogen peroxide and ferrous ion is negligible for wavelengths greater than 300 nm. Consequently,

$$\kappa_{\mathrm{T},\lambda} = \sum_i \alpha_{i,\lambda} C_i \cong \alpha_{\mathrm{Fe(OH)}^{2+}} C_{\mathrm{Fe(OH)}^{2+}} \tag{8}$$

The molar absorptivity of the absorbing species [$\alpha_{Fe(OH)^{2+}}$] as a function of the wavelength was obtained from Faust and Hoigné.[40]

Because the incident UV radiation is polychromatic and the optical properties of the reactants are functions of wavelength, an integration over all the useful wavelengths must be performed. Thus,

$$e^{\mathrm{a}}(x, t) = \int_{\lambda_{\min}}^{\lambda_{\max}} e_\lambda^{\mathrm{a}}(x, t)\, \mathrm{d}\lambda \cong \sum_\lambda e_\lambda^{\mathrm{a}}(x, t) \tag{9}$$

2.2. Experiments. The employed apparatus was a well-mixed tank reactor (Figure 1). The photoreactor was irradiated from the bottom with a black light, mercury arc lamp (Phillips TL 20W/08) placed at the focal axis of a cylindrical reflector of parabolic cross section. The tank was equipped with a thermometer, a liquid sampling valve, and a variable-speed stirrer. The experimental device was connected to a thermostatic bath to facilitate the temperature control. Table 1 presents a summary of the main reactor, lamp, and reflector characteristics and dimensions.

Experimental runs were conducted in the stirred tank photoreactor at pH = 3.0, a ferric ion concentration equal to 1 mM, and three reaction temperatures: 298, 313, and 328 K. Table 2 shows the operating conditions for the Fenton and photo-Fenton

Table 1. Reactor, Lamp, and Reflector Characteristics and Dimensions

	value	units
Reactor		
total liquid volume	3.00×10^{-3}	m^3
diameter	1.42×10^{-1}	m
length	1.89×10^{-1}	m
Lamp Philips TL 20W/08		
nominal power	20	W
output power: 310 nm $\leq \lambda \leq$ 420 nm	2.39	W
diameter	3.70×10^{-2}	m
nominal arc length	6.00×10^{-1}	m
Reflector		
parabola characteristic constant	2.10×10^{-2}	m
distance vertex of parabolic reflector−reactor plate	8.40×10^{-2}	m
length	1.58×10^{-1}	m

Table 2. Operating Conditions for the Experimental Program[a]

	Fenton		photo-Fenton	
temperature (K)	C_P^0/C_F^0	$C_F^0 \times 10^3$ (M)	C_P^0/C_F^0	$C_F^0 \times 10^3$ (M)
298	2.90	2.12	3.05	2.02
	4.87	2.25	5.11	2.21
	8.05	2.13	7.93	2.12
313	3.16	1.99	3.11	2.11
	5.03	2.27	5.20	1.98
	7.95	2.19	7.84	2.08
328	3.11	2.15	2.77	2.18
	4.86	2.23	4.87	2.23
	7.93	2.14	7.74	2.16

[a] Reaction time = 30 min.

experimental program. The experimental procedure began when concentrated sulfuric acid was used to adjust the pH. Then, ferric sulfate solution (Carlo Erba, RPE) was added to the reactor and the reaction temperature adjusted to reach the working conditions. A shutter located between the lamp−reflector system and the bottom of the reactor allowed us to obtain the specified operating conditions. Then, hydrogen peroxide (Carlo Erba, ACS, 30%P) and formic acid (Merck, ACS) solutions were added to the reactor, and the first sample was withdrawn (reaction time equal to zero). Finally, the shutter was removed to start the irradiated experiences.

Runs lasted 30 min, and liquid samples were taken at equal time intervals. As soon as the sample was withdrawn, the Fenton reaction was stopped instantaneously by adding sodium sulfite. Formic acid was analyzed with total organic carbon measurements (Shimadzu TOC-5000A). Concerning the measurement of hydrogen peroxide, a modified iodimetric technique was used. Ferrous ions were tested with absorbance measurements of the Fe(II)−phenantroline complex at 510 nm. In a previous work, it has been experimentally verified that the ferrous ion concentration remains almost constant.[38]

2.3. Evaluation of the Kinetic Parameters. The system of two nonlinear, first-order, ordinary differential equations (eqs 1−9) was numerically solved using a fourth-order Runge−Kutta method. Integration of these equations provides the formic acid and hydrogen peroxide molar concentrations as a function of time. Values of the kinetic parameters K_i ($i = 1-4$) at 298 K were obtained from De Laat and Gallard,[37] and the wavelength-averaged primary quantum yield $\bar{\Phi}$ was taken from Rossetti et al.[38] To obtain the same kinetic parameters at 313 and 328 K we applied a nonlinear regression algorithm,[41] using the proposed kinetic model and the experimental data. Then, with an Arrhenius-type diagram, the corresponding frequency factors (A_i) and activation energies (E_i) were calculated (Table 3).

Table 3. Estimated Values of Activation Energies and Frequency Factors

kinetic parameter	A_i	E_i
K_1	2.23×10^{12} (L mol^{-1} s^{-1})	7.76×10^4 (J mol^{-1})
K_2	4.69×10^{26} (−)	1.66×10^5 (J mol^{-1})
K_3	1.74×10^7 (−)	4.52×10^4 (J mol^{-1})
K_4	3.88×10^{14} (L mol^{-1} s^{-1})	9.90×10^4 (J mol^{-1})

The net radiative flux at the reactor bottom was evaluated with actinometric measurements employing potassium ferrioxalate in an aqueous solution. From these experiments the net radiative flux at the reactor wall was determined to be $q_{wall} = 5.56 \times 10^{-9}$ einstein cm^{-2} s^{-1}.

A set of experimental runs for Fenton and photo-Fenton reactions was performed, using different values of the reaction temperature and of the hydrogen peroxide to formic acid initial molar ratio. Table 2 presents a summary of the operating conditions for the experimental program. Kinetic model and experimental results of formic acid and hydrogen peroxide relative concentrations as a function of time were compared. Figure 2 shows model predictions and experimental data of the time evolution of formic acid and hydrogen peroxide relative concentrations, for a dark and a UV-irradiated solution and for three reaction temperatures: 298, 313, and 328 K. The following operating parameters were also employed for the experimental runs: $C_F^0 \cong 2.2$ mM, $C_P^0/C_F^0 \cong 3$, and $C_{Fe^{3+}} = 1$ mM. Model predictions are compared with experimental data, and a good representation of the formic acid and hydrogen peroxide concentrations is obtained.

Table 4 provides a quantitative comparison between predicted and experimental values of formic acid conversions for Fenton

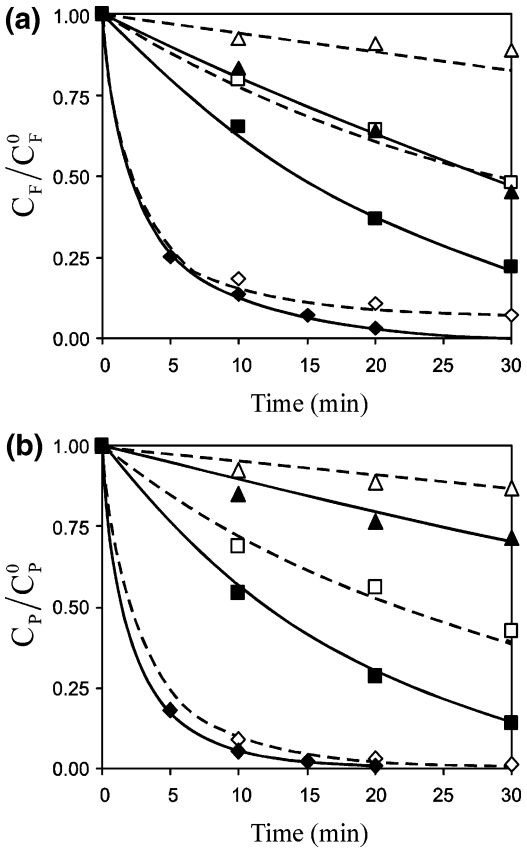

Figure 2. Model and experimental relative concentrations vs time: (a) formic acid, (b) hydrogen peroxide. Key: Fenton (dashed line), photo-Fenton (solid line), 298 K (△, ▲), 313 K (□, ■), 328 K (◇, ◆).

Table 4. Stirred Tank Laboratory Photoreactor: Comparison between Fenton and Photo-Fenton Percent Conversions ($t = 20$ min)

		$C_P^0/C_F^0 = 3$			$C_P^0/C_F^0 = 5$			$C_P^0/C_F^0 = 8$		
temperature (K)		Fenton	photo-Fenton	enhancement (%)	Fenton	photo-Fenton	enhancement (%)	Fenton	photo-Fenton	enhancement (%)
298	experiment	13.5	36.1	167.4	16.4	38.5	134.8	20.6	33.1	60.7
	model	11.9	37.9	218.5	16.1	38.1	136.6	20.2	39.4	95.0
313	experiment	35.6	63.2	77.5	47.3	65.4	38.3	60.0	72.9	21.5
	model	38.7	62.3	61.0	49.3	67.5	36.9	58.5	72.0	23.1
328	experiment	89.3	96.9	11.9	94.8	100.0	5.5	96.8	100.0	3.3
	model	89.8	97.0	8.0	94.3	99.5	5.5	96.7	99.9	3.3

and photo-Fenton reactions, for the complete set of operating conditions employed in the experimental program. Notice that increasing the reaction temperature increases the pollutant conversion for both reactions. Also, it is interesting to note that the photo-Fenton system always produces a formic acid conversion greater than that obtained with the Fenton system: an experimental pollutant conversion enhancement of 167.4% is achieved when the temperature and hydrogen peroxide to formic acid molar ratio are low (298 K and $C_P^0/C_F^0 = 3$). However, a lower increase in the organic pollutant conversion is reached when the reaction temperature and the hydrogen peroxide to formic acid molar ratio are high: only an experimental pollutant conversion enhancement of 3.3% is reached at 328 K and $C_P^0/C_F^0 = 8$.

On the other hand, a hydrogen peroxide to formic acid molar ratio under 3 ($C_P^0/C_F^0 = 0.5$) was studied. For the Fenton process, the formic acid conversions after 20 min are 9.4% at 298 K and 18.9% at 313 K. For the photo-Fenton reaction, the corresponding formic acid conversions are 11.4% at 298 K and 24.8% at 313 K. Thus, pollutant conversion enhancements of 21.3 and 31.2% are achieved at 298 and 313 K, respectively. These results show that the formic acid conversion enhancement cannot be leveled out by temperature when an amount of hydrogen peroxide under the stoichiometric requirement is used.

3. Flat-Plate Solar Reactor

3.1. Reactor model. The experimental device is an isothermal, flat-plate solar photoreactor placed inside the loop of a batch recycling system (Figure 3). The operating conditions of the system may be summarized as follows: (i) a reactor volume smaller than the tank volume, (ii) high recirculating flow rate, and (iii) perfect mixing in the whole recycling system. As it was shown in Rossetti et al.,[42] the mass balance for the formic acid ($i = \mathrm{F}$) and hydrogen peroxide ($i = \mathrm{P}$) are given by

$$\frac{dC_i}{dt} = \frac{V_R}{V_T}\langle R_i(x, t)\rangle_{V_R} + \left(\frac{V_{Tk}}{V_T}\right) R_i^t(t) \quad (i = \mathrm{F, P}) \qquad (10)$$

with the following initial conditions:

$$t = 0 \quad C_i = C_i^0 \quad (i = \mathrm{F, P}) \qquad (11)$$

where V_R, V_{Tk}, and V_T are the reactor, tank, and total liquid volumes, respectively. Notice that the first term on the right-hand side of eq 10 represents the pollutant (or hydrogen peroxide) decomposition rate produced by the photo-Fenton reaction occurring in the irradiated liquid volume, while the second term corresponds to the pollutant (or hydrogen peroxide) degradation rate generated by the thermal reaction that takes place in the nonirradiated liquid volume.

The required reaction rates $R_i(x, t)$ and $R_i^t(t)$ to replace in the solar reactor mass balances (eq 10) are obtained from the kinetic model previously described (eqs 3−6).

To complete the mathematical description of the reactor model, it is necessary to introduce the LVRPA expression on the right-hand side of the kinetic equations (eqs 3 and 5). In a previous work, Rossetti et al.[43] proposed and experimentally verified a rigorous radiation field model for a similar flat-plate solar photoreactor. The authors assumed that only radiation absorption took place in the reacting medium and that the glass window was irradiated with direct and diffuse solar radiation. Then, they computed the LVRPA and the volume-averaged reaction rate of an uranyl oxalate aqueous solution (a well-known chemical actinometer), for different solar zenith angles and actinometer initial concentrations, and compared the predicted results with the experimental decomposition rate data.

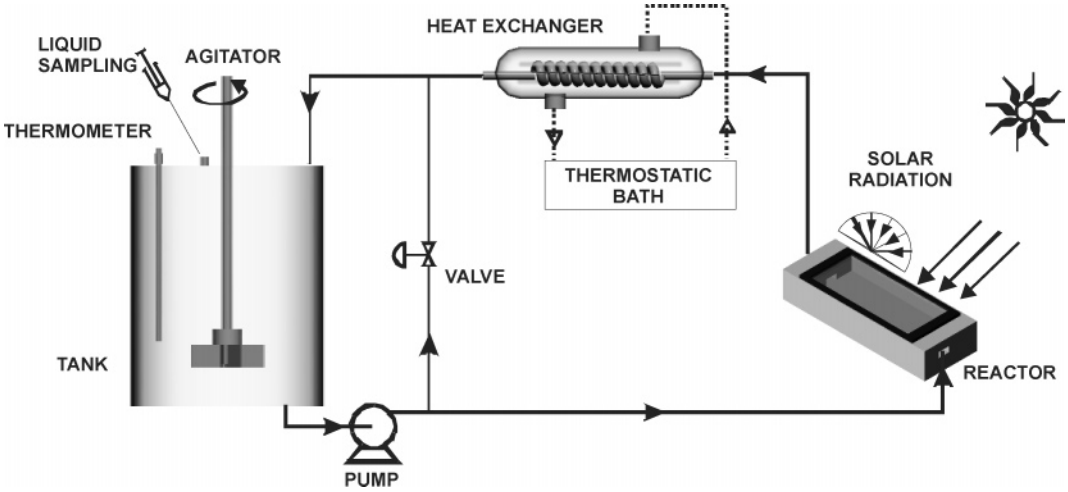

Figure 3. Schematic representation of the flat-plate solar reactor.

In this work, a similar expression is proposed to predict the monochromatic LVRPA as a function of position x inside the solar photoreactor:

$$e^{a}_{\lambda}(x) = \kappa_{\lambda}\left\{ q_{D,\lambda} T_{D,\lambda} \exp(-\kappa_{\lambda} x/\mu_r) + 2 q_{S,\lambda} \frac{n_w^2}{n_a^2} \int_{\mu_{cr}}^{1} T_{S,\lambda} \exp(-\kappa_{\lambda} x/\mu)\, d\mu + 2\rho_B q_{B,\lambda} \left[\int_0^1 \rho_{w-p}(\mu) \exp[-\kappa_{\lambda}(L+x)/\mu]\, d\mu + \int_0^1 \exp[-\kappa_{\lambda}(L-x)/\mu]\, d\mu \right] \right\} \quad (12)$$

Here, $q_{D,\lambda}$ and $q_{S,\lambda}$ are the spectral direct and diffuse solar radiation incidents on the glass window of the reactor, $q_{B,\lambda}$ is the spectral net radiation flux reaching the reactor bottom, $T_{D,\lambda}$ and $T_{S,\lambda}$ are the direct and diffuse transmittances, κ_{λ} is the spectral volumetric absorption coefficient of the absorbing species, L is the reactor depth, ρ_B the reactor bottom reflectivity, ρ_{w-p} is the water−plate reflectivity, and $\mu = \cos\theta$. In eq 12 we have also defined

$$T_{D,\lambda} = \frac{[1-\rho_{a-p}(\mu^*_{in})][1-\rho_{p-w}(\mu_r')]\tau_{\lambda}(\mu_r')}{1-\tau_{\lambda}^2(\mu_r')\rho_{a-p}(\mu_r')\rho_{p-w}(\mu_r')} \quad (13)$$

$$T_{S,\lambda} = \frac{[1-\rho_{a-p}(\mu^*)][1-\rho_{p-w}(\mu')]\tau_{\lambda}(\mu')}{1-\tau_{\lambda}^2(\mu')\rho_{a-p}(\mu')\rho_{p-w}(\mu')} \quad (14)$$

$$\tau_{\lambda}(\mu') = \exp\left(-\kappa_{p,\lambda}\frac{e}{\mu'}\right) \quad (15)$$

In eqs 13−15 ρ_{a-p} and ρ_{p-w} are the air−plate and plate−water reflectivities, respectively, $\kappa_{p,\lambda}$ is the spectral volumetric absorption coefficient of the glass plate, and e is the glass plate thickness. More details on the modeling and experimental verification of the radiation field inside of the flat-plate solar reactor can be found elsewhere.[43]

3.2. Experiments. The experimental device was a well-stirred, flat-plate solar reactor placed inside a batch recycling system (Figure 3). The frame of the reactor was made of Nylon and, at the reactor top, a window made of Tempax glass was placed. A tank of Pyrex glass and a centrifugal pump (Vanton Flex-I-Liner) completed the system. To keep the reaction temperature constant, the apparatus had an all-glass heat exchanger connected to a thermostatic bath (Lauda K2R). The heat exchanger and the high recirculating flow rate of the aqueous solution favored the temperature control of the reacting mixture. Values of the solar reactor and optical parameters can be found elsewhere.[42]

The experimental procedure began when concentrated sulfuric acid was added to the mixture of ferric sulfate (Carlo Erba, RPE) and hydrogen peroxide (Carlo Erba, ACS, 30%P) in water to adjust the pH at 3.0. During the initial period of each experimental run, the reactor window was covered with an opaque paper to avoid solar radiation entrance. Then, the formic acid solution was added to the tank and the opaque paper was removed; this operation determined the starting time of the photo-Fenton reaction. Experimental runs were carried out during 30 min, and the liquid sampling operation was repeated at equal time intervals until the run was concluded. Formic acid, hydrogen peroxide, and ferrous ion were analyzed with the procedure described in section 2.2.

Table 5. Measured and Predicted UV Solar Radiation

temperature (K)	time (min)	zenith angle (deg)	UV solar radiation (W m^{-2})		error (%)
			measurement	prediction	
298	0	10.5	37.6	38.3	2.0
	10	9.4	37.6	38.5	2.3
	20	8.8	37.8	38.6	2.0
	30	8.7	37.9	38.6	1.9
313	0	11.3	38.0	38.2	0.6
	10	9.9	38.1	38.5	1.0
	20	8.9	39.0	38.6	0.9
	30	8.3	39.3	38.7	1.4
328	0	11.5	37.8	38.2	1.1
	10	10.2	38.2	38.5	0.8
	20	9.1	38.4	38.7	0.6
	30	8.5	39.0	38.7	0.7

3.3. Predicted and Experimental Results. To evaluate $q_{D,\lambda}$ and $q_{S,\lambda}$ at the Earth's surface for cloudless atmospheres, we have applied the model proposed by Bird and Riordan.[44] For each one of the experimental runs, UV solar radiation predictions obtained with the Bird and Riordan's model were compared with the broadband UV solar radiation incident on the reactor glass window. Solar radiation measurements at equal time intervals were made by means of a Kipp and Zonen CUV3 radiometer. Table 5 presents values of measured and predicted ultraviolet solar radiation incident at the reactor window, for experimental runs carried out at the reaction temperatures 298, 313, and 328 K. For each reaction time, the corresponding values of the zenith angle (column 3) and the percentage error (column 6) were also added. It can be observed that the maximum relative error between predicted radiation fluxes and experimental measurements is not higher than 2.3%. In addition, it should be noted that the maximum variation of the measured UV solar radiation incident on the glass window of the reactor for each one of the experimental runs is not higher than 3.3%. Accordingly, a time-averaged solar zenith angle could be used for the numerical solution of the solar radiation model.[42]

Model predictions of formic acid and hydrogen peroxide concentrations as a function of time were obtained solving the system of nonlinear, first order, ordinary differential equations (eqs 10 and 11), the equations for the computation of the spectral LVRPA (eqs 12−15), and the expressions of the Bird and Riordan model[44] for the evaluation of the direct and diffuse spectral solar radiation incident at the reactor window. Formic acid and hydrogen peroxide reaction rates were computed using the temperature-dependent kinetic model (eqs 3−6).

Figure 4 shows solar reactor model and experimental results of the relative concentrations C_F/C_F^0 and C_P/C_P^0 as a function of time, for the Fenton and photo-Fenton processes and for 298, 313, and 328 K. Constant values of $C_F^0 = 2.2$ mM, $C_{Fe^{3+}} = 1$ mM, $C_P^0/C_F^0 = 3$, and the time-averaged solar zenith angle $\langle\theta_Z\rangle = 9.5°$ were used. A good agreement between model predictions and experimental points may be observed. Notice that for formic acid relative concentrations greater than 0.1 and hydrogen peroxide relative concentrations greater than 0.03, the relative error is not higher than 8%.

Table 6 shows a quantitative comparison between theoretical and experimental results of the pollutant conversion after 20 min of reaction time. In this case, it can be observed again that when increasing the reaction temperature, the formic acid conversion for Fenton and photo-Fenton reactions increases too. It should be noted as well that UV solar radiation improves the effectiveness of the Fenton system. However, an important result is that at higher values of the reaction temperature, the enhancement of the pollutant conversion is less important. For

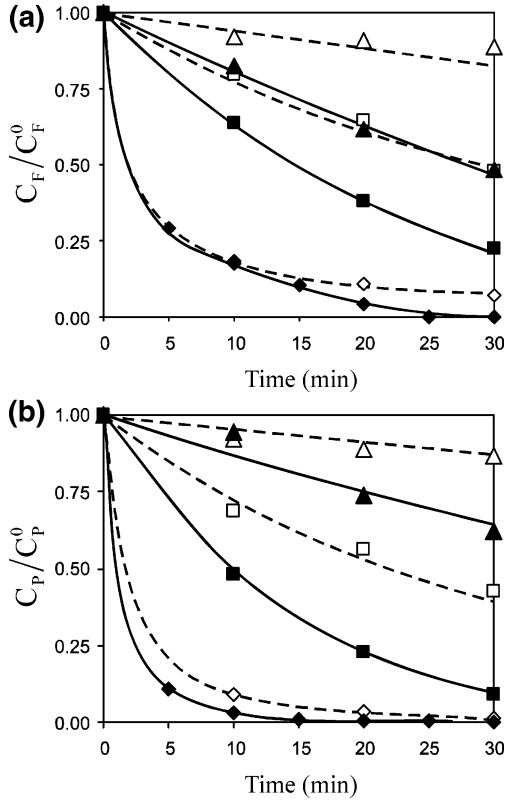

Figure 4. Model and experimental relative concentrations vs time: (a) formic acid, (b) hydrogen peroxide. Key: Fenton (dashed line), photo-Fenton (solid line), 298 K (△, ▲), 313 K (□, ■), 398 K (◇, ◆).

Table 6. Flat-Plate Solar Reactor: Comparison between Fenton and Photo-Fenton Percent Conversions (t = 20 min)

temperature (K)		Fenton	photo-Fenton	enhancement (%)
298	experiment	13.5	38.5	186.0
	model	11.9	37.8	217.5
313	experiment	35.6	61.9	74.0
	model	38.7	61.6	59.4
328	experiment	89.2	95.8	7.4
	model	89.8	95.1	5.8

example, experimental conversion enhancements of 186.0, 74.0, and 7.4% are achieved at 298, 313, and 328 K, respectively.

4. Conclusions

A reactor model was developed to study the temperature effects on the degradation of formic acid for Fenton and photo-Fenton processes. Frequency factors and activation energies between 298 and 328 K were estimated for both reactions, employing a well-stirred tank laboratory photoreactor irradiated from the bottom. The kinetic model was afterward used to predict formic acid and hydrogen peroxide concentrations as a function of time in a flat-plate solar reactor placed inside a batch recycling system.

Predictions of the solar reactor model were compared with experimental data, and a satisfactory representation of the formic acid and hydrogen peroxide concentrations versus time data was observed. For formic acid relative concentrations greater than 0.1 and hydrogen peroxide relative concentrations greater than 0.03, the maximum deviation was not higher than 8%.

Model predictions and experimental data show that UV solar irradiation improves the effectiveness of the Fenton process. We found that, when the temperature is low (298 K), the formic acid conversion enhancement after 20 min of reaction time is significantly increased (186.0%). Nevertheless, for the highest temperature investigated in this work (328 K), this effect is less important (7.4%).

Acknowledgment

The authors are grateful to Universidad Nacional del Litoral, Consejo Nacional de Investigaciones Científicas y Técnicas, and Agencia Nacional de Promoción Científica y Tecnológica for their support to produce this work. They also thank Eng. Claudia M. Romani for technical assistance.

Nomenclature

A_i = frequency factor, $m^3\ mol^{-1}\ s^{-1}$ (A_1 and A_4), dimensionless (A_2 and A_3)
C = molar concentration, $mol\ m^{-3}$
E_i = activation energy, $J\ mol^{-1}$
e = plate thickness, m
e^a = local volumetric rate of photons absorption (LVRPA), einstein $m^{-3}\ s^{-1}$
f_λ = normalized spectral distribution of the lamp output power, dimensionless
K_i = kinetic parameter, $m^3\ mol^{-1}\ s^{-1}$ (K_1 and K_4), dimensionless (K_2 and K_3)
L = reactor depth, m
n = refractive index, dimensionless
q = net radiative flux, einstein $m^{-2}\ s^{-1}$
R = reaction rate, $mol\ m^{-3}\ s^{-1}$
t = time, s
T = transmittance, dimensionless
V = volume, m^3
x = spatial coordinate, m
$\mathbf{x}$ = vector representing position in a 3D space, m

Greek Letters

α = molar absorptivity, $m^2\ mol^{-1}$
θ = spherical coordinate, rad
θ_z = solar zenith angle, deg
κ = volumetric absorption coefficient, m^{-1}
λ = wavelength, nm
μ = the quantity cos θ, dimensionless
ρ = reflectivity
Φ = primary quantum yield, $mol\ einstein^{-1}$
τ = variable defined in eq 15, dimensionless

Subscripts

a = air property
B = reactor bottom property
cr = critical value
D = direct radiation
F = relative to formic acid
Fe^{2+} = relative to ferrous ion
Fe^{3+} = relative to ferric ion
in = incident radiation
p = plate property
P = relative to hydrogen peroxide
r = refracted radiation
R = reactor property
S = diffuse radiation
Tk = tank property
w = water solution property
wall = wall property
λ = indicates a dependence on wavelength

Superscripts

0 = initial condition
t = thermal rate

* = air property
′ = glass plate property

Special Symbols

⟨...⟩ = average value over a defined space
$\overline{...}$ = averaged value over the wavelength interval

Literature Cited

(1) Nogueira, R. F. P.; Guimaráes, J. R. Photodegradation of Dichloroacetic Acid and 2,4-Dichlorophenol by Ferrioxalate/H_2O_2 System. *Water Res.* **2000**, *34*, 895.

(2) Muñoz, I.; Rieradevall, J.; Torrades, F.; Peral, J.; Domènech, X. Environmental Assessment of Different Advanced Oxidation Processes Applied to a Bleaching Kraft Mill Effluent. *Chemosphere* **2006**, *62*, 9.

(3) Andreozzi, R.; D'Apuzzo, A.; Marotta, R. A. Kinetic Model for the Degradation of Benzothiazole by Fe^{+3}-Photo-Assisted Fenton Process in a Completely Mixed Batch Reactor. *J. Hazard. Mat.* **2000**, *B80*, 241.

(4) Arslan, I.; Balcioglu, I. A.; Bahnemann, D. W. Advanced Chemical Oxidation of Reactive Dyes in Simulated Dyehouse Effluents by Ferrioxalate-Fenton/UV-A and TiO_2/UV-A Processes. *Dyes Pigm.* **2000**, *47*, 207.

(5) Dillert, R.; Huppatz, J.; Renwrantz, A.; Siebers, U.; Bahnemann, D. Light-Induced Degradation of Nitroaromatic Compounds in Aqueous Systems: Comparison between Titanium Dioxide Photocatalysis and Photo-Fenton Reactions. *J. Adv. Oxid. Technol.* **1999**, *4*, 85.

(6) Huston, P. L.; Pignatello, J. J. Reduction of Perchloroalkanes by Ferrioxalate-Generated Carboxylate Radical Preceding Mineralization by the Photo-Fenton Reaction. *Environ. Sci. Technol.* **1996**, *30*, 3457.

(7) Pignatello, J.; Sun, Y. Complete Oxidation of Metolachlor and Methyl Parathion in Water by the Photoassisted Fenton Reaction. *Water Res.* **1995**, *29*, 1837.

(8) Katsumata, H.; Kaneco, S.; Suzuki, T.; Ohta, K.; Yobico, Y. Photo-Fenton Degradation of Alachlor in the Presence of Citrate Solution. *J. Photochem. Photobiol. A. Chem.* **2006**, *180*, 38.

(9) Emilio, C. A.; Jardim, W. F.; Litter, M. I.; Mansilla, H. D. EDTA Destruction Using the Solar Ferrioxalate Advanced Oxidation Technology (AOT). Comparison with Solar Photo-Fenton Treatment. *J. Photochem. Photobiol., A* **2002**, *151*, 121.

(10) Gernjak, W.; Krutzler, T.; Glaser, A.; Malato, S.; Caceres, J.; Bauer, R.; Fernández-Alba, A. R. Photo-Fenton Treatment of Water Containing Natural Phenolic Pollutants. *Chemosphere* **2003**, *50*, 71.

(11) Rodríguez, M.; Malato, S.; Pulgarin, C.; Contreras, S.; Curcó, D.; Giménez, J.; Esplugas, S. Optimizing the Solar Photo-Fenton Process in The Treatment of Contaminated Water. Determination of Intrinsic Kinetic Constants for Scale-Up. *Sol. Energy* **2005**, *79*, 360.

(12) Hincapié Pérez, M.; Peñuela, G.; Maldonado, M. I.; Malato, O.; Fenández-Ibáñez P.; Oller, I.; Gernjak, W.; Malato, S. Degradation of Pesticides in Water Using Solar Advanced Oxidation Proceses. *Appl. Catal., B* **2006**, *64*, 272.

(13) Malato, S.; Blanco, J.; Vidal, A.; Alarcón, D.; Maldonado, M.; Cáceres, J.; Gernjak, W. Applied Studies in Solar Photocatalytic Detoxification: an Overview. *Sol. Energy* **2003**, *75*, 329.

(14) Maldonado Rubio, M. I.; Gernjak, W.; Oller Alberola, I.; Blanco Gálvez, J.; Fernández-Ibáñez, P.; Malato Rodríguez, S. Photo-Fenton Degradation of Alachlor, Atrazine, Chlorfenvinphos, Diuron, Isoproturon and Pentachlotophenol at Solar Pilot Plant. *Int. J. Environ. Pollut.* **2006**, *27*, 135.

(15) Amat, A. M.; Arques, A.; Miranda, M. A.; Seguí, S. Photo-Fenton Reaction for Abatement of Commercial Surfactants in a Solar Pilot Plant. *Sol. Energy* **2004**, *77*, 559.

(16) Pérez-Estrada, L. A.; Malato, S.; Gernjak, W.; Agüera, A.; Thurman, M. E.; Ferrer, I.; Fernández-Alba, A. R. Photo-Fenton Degradation of Diclofenac: Identification of Main Intermediates and Degradation Pathway. *Environ. Sci. Technol.* **2005**, *39*, 8300.

(17) Nogueira, R. F. P.; Silva, M. R. A.; Trovó, A. G. Influence of the Iron Source on the Solar Photo-Fenton Degradation of Different Classes of Organic Compounds. *Sol. Energy* **2005**, *79*, 384.

(18) Lee, Y.; Lee, C.; Yoon, J. High Temperature Dependence of 2,4-Diclorophenoxyacetic Acid Degradation by Fe^{3+}/H_2O_2 System. *Chemosphere* **2003**, *51*, 963.

(19) López, A.; Mascolo, G.; Detomaso, A.; Lovecchio, G.; Villani, G. Temperature Activated Degradation (Mineralization) of 4-Chloro-3-Metyl Phenol by Fenton's Reagent. *Chemosphere* **2005**, *59*, 397.

(20) Rodríguez, M. L.; Timokhin, V. I.; Contreras, S.; Chamarro, E.; Esplugas, S. Rate Equation for the Degradation of Nitrobenzene by 'Fenton-Like' Reagent. *Adv. Environ. Res.* **2003**, *7*, 583.

(21) Malik, P.; Saha, S. Oxidation of Direct Dyes with Hydrogen Peroxide Using Ferrous Ion as Catalyst. *Sep. Purif. Technol.* **2003**, *31*, 241.

(22) Gulkaya, I.; Surucu, G. A.; Dilek, F. B. Importance of H_2O_2/Fe^{2+} Ratio in Fenton's Treatment of a Carpet Dyeing Wastewater. *J. Hazard. Mater.* **2006**, *B136*, 763.

(23) Arslan, I.; Teksoy, S. Acid Dyebath Effluent Pretreatment Using Fenton's Reagent: Process Optimization, Reaction Kinetics and Effects on Acute Toxicity. *Dyes Pigm.* **2007**, *73*, 31.

(24) Bacardit, J.; Hultgren, A.; Garcia-Molina, V.; Esplugas, S. Biodegradability Enhancement of Wastewater Containing 4-Chlorophenol by Means of Photo-Fenton. *J. Adv. Oxid. Technol.* **2006**, *9*, 27.

(25) Durán, A.; Monteagudo, J. M.; Mohedano, M. Neuronal Networks Simulation of Photo-Fenton Degradation of Reactive Blue 4. *Appl. Catal., B* **2006**, *65*, 127.

(26) Al Momani, F. Impact of Photo-Oxidation Technology on the Aqueous Solutions of Nitrobenzene: Degradation Efficiency and Biodegradability Enhancement. *J. Photochem. Photobiol., A* **2006**, *179*, 184.

(27) Rodriguez, M.; Sarría, V.; Esplugas, S.; Pulgarin, C. Photo-Fenton Treatment of a Biorecalcitrant Wastewater Generated in Textile Activities: Biodegradability of the Photo-Treated Solution. *J. Photochem. Photobiol., A* **2002**, *151*, 129.

(28) Jain, D. M. Photo Fenton Degradation for Environmental Application. *J. Ind. Pollut. Control* **2005**, *21*, 181.

(29) Lee, C.; Yoon, J. Temperature Dependence of Hydroxyl Radical Formation in the *hν*/Fe^{3+}/H_2O_2 and Fe^{3+}/H_2O_2 Systems. *Chemosphere* **2004**, *56*, 923.

(30) Gernjak, W.; Fuerhacker, M.; Fernández-Ibañez, P.; Blanco, J.; Malato, S. Solar Photo-Fenton Treatment-Process Parameters and Process Control. *Appl. Catal., B* **2006**, *64*, 121.

(31) Torrades, F.; Pérez, M.; Mansilla, H. D.; Peral, J. Experimental Design of Fenton and Photo-Fenton Reactions for the Treatment of Cellulose Bleaching Effluents. *Chemosphere* **2003**, *53*, 1211.

(32) Pérez, M.; Torrades, F.; Domènech, X.; Peral, J. Fenton and Photo-Fenton Oxidation of Textile Effluents. *Water. Res.* **2002**, *36*, 2703.

(33) Malato, S.; Blanco, J.; Maldonado, M. J.; Fernández, P.; Gernjak, W.; Oller Alberola, I. Treatment of Chlorinated Solvents by TiO_2 Photocatalysis and Photo-Fenton: Influence of Operating Conditions in a Solar Pilot Plant. *Chemosphere* **2005**, *58*, 391.

(34) Sagawe, G.; Lehnard, A.; Lübber, M.; Bahnemann, D. The Insulated Solar Fenton Hybrid Process: Fundamental Investigations. *Helv. Chim. Acta* **2001**, *84*, 3742.

(35) Sarria, V.; Kenfack, S.; Malato, S.; Blanco, J.; Pulgarin, C. New Helio-Photocatalytic-Photovoltaic Hybrid System for Simultaneous Water Decontamination and Solar Energy Conversion. *Sol. Energy* **2005**, *79*, 353.

(36) Pignatello, J. J. Dark and Photoassisted Fe^{+3}-Catalyzed Degradation of Chlorophenoxy Herbicides by Hydrogen Peroxide. *Environ. Sci. Technol.* **1992**, *26*, 944.

(37) De Laat, J.; Gallard, H. Catalytic Decomposition of Hydrogen Peroxide by Fe(III) in Homogeneous Aqueous Solution: Mechanism and Kinetic Modeling. *Environ. Sci. Technol.* **1999**, *33*, 2726.

(38) Rossetti, G. H.; Albizzati, E. D.; Alfano, O. M. Decomposition of Formic Acid in Water Solution Employing the Photo-Fenton Reaction. *Ind. Eng. Chem. Res.* **2002**, *41*, 1436.

(39) Alfano, O. M.; Romero, R. L.; Cassano, A. E. A Cylindrical Photoreactor Irradiated from the Bottom. I. Radiation Flux Density Generated by a Tubular Source and a Parabolic Reflector. *Chem. Eng. Sci.* **1985**, *40*, 2119.

(40) Faust, B. C.; Hoigné, J. Photolysis of Fe(III)-Hydroxy Complexes as Sources of OH Radicals in Clouds, Fog and Rain. *Atmos. Environ.* **1990**, *24A*, 79.

(41) Marquardt, D. An Algorithm for Least-Squares Estimation of Nonlinear Parameters. *SIAM J. Appl. Math.* **1963**, *11*, 431.

(42) Rossetti, G. H.; Albizzati, E. D.; Alfano, O. M. Modeling of a Flat-Plate Solar Reactor. Degradation of Formic Acid by the Photo-Fenton Reaction. *Sol. Energy* **2004**, *77*, 461.

(43) Rossetti, G.; Albizzati, E.; Alfano, O. Modeling and Experimental Verification of a Flat-Plate Solar Photoreactor. *Ind. Eng. Chem. Res.* **1998**, *37*, 3592.

(44) Bird, R. E.; Riordan, C. Simple Solar Spectral Model for Direct and Diffuse Irradiance on Horizontal and Tilted Planes at the Earth's Surface for Cloudless Atmospheres. *J. Clim. Appl. Meteorol.* **1986**, *25*, 87.

Received for review January 6, 2007
Revised manuscript received March 22, 2007
Accepted March 23, 2007

IE0700258